Final Draft
of the original manuscript:

Stanev, E.V.; Peneva, E.; Chtirkova, B.:
Climate change and regional ocean water mass disappearance: Case of the Black Sea
In: Journal of Geophysical Research : Oceans (2019) AGU

DOI: 10.1029/2019JC015076

Climate change and regional ocean water mass disappearance: Case of the Black Sea

Emil V. Stanev[1, 2], Elisaveta Peneva[3], Boriana Chtirkova[3]

[1]Institute of Coastal Research, Helmholtz-Zentrum Geesthacht, Geesthacht, Germany
[2]Research Department, University of Sofia, Sofia, Bulgaria
[3]Department of Meteorology and Geophysics, University of Sofia, Sofia, Bulgaria

Abstract

Data from profiling floats reveal that climate change in the Black Sea leads to the disappearance of specific water masses. The observed thermohaline change is possibly an amplified precursor of the changes to expect in the greater oceans. The warming trend in the cold intermediate layer (CIL) of ~0.05°C/yr was more than double the trend in previous decades, and its temperature approached that of the waters in the deeper layers (~9°C), which signified its disappearance. This evolution was due to the warmer winters over the last fourteen years. Intermittent major cold water formation events (only three during this period) could not sufficiently refill the CIL. A "density constriction" (minimum spread of density) was found at ~14.25 σ_t, and it separated two thermohaline regimes: temperature-dominated above and salinity-dominated beneath. Below this depth, the CIL is seen as a "corner" in the T-S diagram at ~18 salinity and ~9°C, where the profiles make a curve. The variability in the T-S relationships at given σ_t levels in the CIL revealed trends dominated by diapycnic mixing with deeper layers (the high-salinity pool acts as a source of salt for the upper ocean). After 2010, salinity anomalies started to occur rhythmically with increasing amplitudes at the depths of the CIL. In the absence of a pronounced CIL in recent years, the relative role of salinity variability in the thermohaline state of the upper layers increased. Further trends and the plausibility of similar events in other similar environments are also addressed.

1. Introduction

Water masses give a very robust representation of the thermohaline state of the ocean and ocean circulation. Analysis of their formation and transformation enables us to identify the dominant processes controlling the planetary climate and the most important regional oceanographic characteristics. Regional seas, although very small compared to the ocean basins, also show pronounced thermohaline characteristics, which largely differ from basin to basin. Because of their smaller size and specific combinations of bathymetry, forcing factors and responses, regional or almost enclosed seas could provide sensitive cases helping us to

decipher responses to regional climate change, e.g., the disappearance of certain water masses, which is still not easy to observe in the recent changes in water masses globally.

The Black Sea is almost enclosed and neighbors a major catchment area spread across the continent (1874,904 km^2 against surface area of 436,400 km^2). This water body shows extremely stable vertical stratification, and its water density changes from ~1011 kg/m^3 at the ocean surface to ~1016 kg/m^3 at 100 m depth. This large gradient is maintained by the balance between buoyancy fluxes. The major fluxes are represented by river runoff and Mediterranean inflow, with the latter entering the Black Sea through the Bosporus Strait. The basin-wide thermal buoyancy flux is approximately four times smaller than the haline buoyancy flux (Stanev et al., 2003). However, the amplitude of the seasonal thermal buoyancy flux exceeds that of the haline buoyancy flux by an order of magnitude. This contrast leads to the following concept: the mean thermohaline state in the Black Sea is dominated by the water and salinity balance (dilution at the surface and salinification by the Mediterranean inflow); air-sea heat exchange shapes the seasonal variability.

Winter cooling, which is an essential element of the seasonal variability, is too weak to overcome the stable salinity (density) stratification over large depth intervals; thus, the pycnocline sets the depth of penetration of the seasonal signal, which is not more than ~100-150 m. Therefore, the Black Sea is characterized by a small depth interval of thermo-haline inertia and a large sensitivity to surface fluxes. This situation is quite different from the cases of other semienclosed (but weakly stratified) systems, e.g., the Gulf of Lion in the Mediterranean, where convection is deep (Schott et al., 1996). The major consequence of the shallow convection in the Black Sea is the formation of a cold intermediate layer (CIL) extending over the whole basin area. In its core, the temperature during the warm part of the year is lower than the temperatures at the surface and in the deeper layers. At present, the CIL is considered a permanent feature in the Black Sea vertical stratification and is classified as a water mass. The positions of the 8°C isotherms have traditionally been considered the lower and upper boundaries of the CIL (Blatov et al., 1984; Ozsoy and Unluata, 1997).

Two ventilation mechanisms that affect the physical and biogeochemical systems in the Black Sea differently must be distinguished: one mechanism brings cold and oxygen-rich water from above (e.g., due to winter convection), and the other mechanism brings warmer and oxygen-rich water from the Bosporus (intermittently but during the whole year; Jarosz et al.,

2011; Stanev et al., 2017). In brief, the cold intermediate water (CIW) mass formation provides the ventilation mechanism in the upper ocean; the Bosporus plume ventilates layers below the CIL (Falina et al., 2017; Stanev et al., 2018). The very low rate of ventilation of deep layers explains the physical reasons for the permanent anoxic conditions that characterize depths below 100-150 m. In this work, we address the first mechanism, that is, the formation of cold water.

In the past, most physical oceanographers accepted the hypothesis of Kolesnikov (1953) that the advection of very cold waters from the northwest shelf provided the major contribution to the formation of the CIL. Currently, oceanographers accept that the seasonal replenishment of the CIL is subject to a number of important processes, such as local cooling, slope convection, interaction with open ocean eddies and persistent coastal anticyclonic eddies, and vertical mixing (Ovchinnikov and Popov, 1987; Oguz and Besiktepe, 1999; Stanev and Staneva, 2001; Gregg and Yakushev, 2005; Shapiro et al., 2010, 2011; Piotukh et al., 2011; Korotaev et al., 2014; Capet et al., 2014; Ostrovskii and Zatsepin, 2016; Mihailov et al, 2016; Akpinar et al., 2017). The quantification of regional water mass formation by Stanev et al. (2003) demonstrated a strong regional dependence as well as a substantial contribution from the open ocean areas to the total amount of water injected into the CIL.

The replenishment time of the CIL is ~5 years (Ovchinnikov, 1998; Lee et al. 2002; Stanev et al., 2003). The fact that the CIW does not disappear during the warm part of the year is explained by the low vertical turbulent exchange in the Black Sea (coefficients of approximately $1–4\times10^{-6}$ m^2 s^{-1}), approaching the values of molecular exchange (Lewis and Landing, 1991; Stanev et al., 1997; Gregg and Yakushev, 2005). These low values are caused by either strong summer temperature stratification in the upper layer (reducing the mixing with the surface layers) or by strong stratification in the halocline (reducing the mixing with the deeper layers). The CIL remains “sandwiched” (encapsulated) between the upper mixed layer and the pycnocline. The CIL refills in the winter and does not disappear in the summer; thus, it exists permanently according to historical data.

Acting as a buffer between the surface layers and the pycnocline, the CIL “integrates” information from atmospheric forcing over a longer time. Data analyses thus decipher interannual and longer-term sustainable trends (Konovalov et al., 2005; Oguz et al., 2006; Piotukh, et al., 2011; Capet et al., 2016). Different hypotheses are possible about the effect of

103 global and regional climate change in the Black Sea. Warming could result in (1) a reduction
104 in the volume of convected waters because of warmer winters; (2) a change in the stabilizing
105 effect of salinity due to alterations in the water and salt balance caused by differences in
106 evaporation and precipitation; (3) a change in wind conditions, which currently oppose the
107 stabilizing role of salinity but could affect the structure of surface and intermediate layers; and
108 (4) a modification of the water exchange between the Black Sea and the Mediterranean by
109 changing wind conditions (Jarosz et al., 2011; Stanev et al., 2017). The large number of
110 possible feedback mechanisms makes expectations based on simple considerations difficult.
111
112 The modulation of the cold water content in the CIL by year-to-year variability and longer-
113 term trends has been studied by Staneva and Stanev (2002) and Miladinova et al. (2017), who
114 used numerical models; however, the model-estimated trends need further validation.
115 Analyses of the thermohaline state for long periods based on measurements are also difficult
116 because of data availability. The interpretation of long-term changes in the Black Sea from
117 observational data can be biased by the poor coverage of data in space and time (Stanev et al.,
118 2013). This problem seems to have been solved in the era of Argo floats, which have provided
119 continuous observations in the Black Sea for more than a decade. This period is sufficient to
120 revisit the dynamics of the CIL with a focus on its longer-term evolution. One additional
121 motivation for this work stems from our previous analyses (Stanev et al., 2013; 2017), which
122 demonstrate a substantial warming of the CIL compared to the historical data. Currently,
123 temperature values in the CIL as low as those defined by Blatov et al. (1984) are rare.
124
125 In comparison to the works of Konovalov et al. (2005), Oguz et al. (2006) and Capet et al.
126 (2016), who addressed longer-term changes in physical and biogeochemical systems in the
127 Black Sea using historical data, we (1) analyze a shorter period for which a continuous data
128 set from Argo floats is available, (2) focus on the disappearance of the CIL during 2015-2017
129 and its intermittent replenishment, and (3) elucidate the correlation between salinity and
130 temperature, which is focused on the T-S analysis of water masses. We use almost the same
131 data as Akpinar et al. (2017), which extend until the present time. However, unlike the study
132 of these authors, who analyzed the observations from individual floats for the periods of
133 operation at their specific observing locations, we give less weight to the regional
134 characteristics, focusing on the trends in the full data set. This approach is justified,
135 particularly because the analysis of observations in density coordinates reduces the scatter of
136 data caused by regional conditions and gives an overall view of the temporal variability of the

vertical structure of the Black Sea water mass. The interrelationship between temperature and salinity and the consequent changes in the T-S characteristics are demonstrated to serve as important indicators of the change in the Black Sea water mass. By investigating this relationship, we provide a robust estimate of the evolution of the Black Sea state over the last ~14 years. The conditions beyond which the CIL will disappear are also addressed.

The paper is structured as follows: we first describe the data in section 2, which is followed by an analysis of forcing in section 3, the temporal variability of the CIL and its replenishment in section 4, a T-S analysis in section 5, discussion and conclusions.

2. Data

At the end of the 20th to the beginning of the 21st century, the Argo program for ocean monitoring was initiated with the objective of delivering regular information about the state of the ocean water column down to 2000 m depth. From 2005 to the present, 38 Argo floats have been deployed in the Black Sea (Korotaev et al., 2006; Stanev et al., 2013; Grayek et al., 2015). In some periods, more than ten floats have operated at the same time, which is impressive for this small basin (see inset in Fig. 1 and Supporting information, Fig. S1, S2, S3). The northwestern shelf part of the Black Sea is not visited by the Argo floats (Fig. 1) because of its shallow depths. In the present study 33 floats are used, which measured 5884 profiles in total. Five floats are not included in the analysis because they operated for a very short time or did not operate properly. The above-cited publications provide further methodological details. The technical details about the profilers used here are given in Supporting Information.

Compared with historical observations, most of which were performed during the warm part of the year, the sampling provided by the Argo missions is rather uniform during the individual seasons (Fig. S2). The vertical distribution of seasonal mean profiles (insets in Fig. S2) demonstrates a well-known vertical structure: a two-layer system with the main pycnocline at approximately 100-300 m, a strong seasonal thermocline and a CIL at the upper part of the halocline. The seasonal thermocline and the CIL, which are not well represented in the depth range 0-1500 m because the upper layer in the Black Sea is very thin, are addressed in the following with more detail for the upper ~250 m.

3. Forcing and response

3.1 Meteorological forcing

The variability of the CIL is largely dependent on meteorological forcing (Stanev et al., 2003; Oguz et al., 2006; Piotukh, et al., 2011); therefore, before addressing the evolution of oceanographic conditions, we first present the meteorological situation during the period of observations. Two data sets were used: the regional observations of surface air temperature at station Varna (the station is 43 m above sea level; see Fig. 1 for its location) and surface air temperature from model reanalysis using the ERA-5 data set (Fig. 2a). From the latter data set, a location in the interior Black Sea was selected (symbol E in Fig. 1), which was representative of the open ocean.

The changes in the cold water masses followed the changes in the severity of individual winters. The latter were characterized by the absolute temperature minima and the length of periods with cold temperatures. These characteristics were better pronounced in the coastal data, as shown by the thin gray line in Fig. 2a, in the years 2006, 2010 and 2012, when the air temperature at the Varna station decreased below -12°C. No such cold temperatures have been measured since then.

The annual mean temperatures did not change much; however, changes in the winter temperatures were more pronounced. The monthly mean temperature of the coldest month in the open sea was below 0°C only during 2006, 2012 and 2017 (Fig. 2b). Section 4 will show that these were the years when the CIL refilled with cold water. The coldest monthly mean temperature at station Varna ranged substantially (between -1°C and 6°C) with warm phases prevailing. The sensitivity of heat fluxes over the Black Sea to the surface air temperature (Staneva and Stanev, 1998; Schrum et al., 2001) suggests that this persistence of warm winters could explain the recent changes of water mass formation in the Black Sea (see section 4). This finding is consistent with a similar conclusion made by Kniebusch et al. (2019), who showed that in the Baltic Sea, which has a similar system to the Black Sea, most of the SST variability could be explained by the surface air temperature.

3.2 Vertical structure of the upper layers

With the unique data set collected by the Argo floats, the representation of the basic characteristics of the Black Sea stratification (Fig. 3) appeared much more credible than those in previous studies, which reflected problems in interpreting observations that were non-

homogeneous in time and space. In the upper mixed layer, the high surface temperatures in summer led clear decreases in density (Fig. 3c mirrors Fig. 3a at the surface). The individual vertical profiles in this layer in the low-temperature interval between 6 and 9°C illustrate separate convection events.

The convergence of density profiles at ~40 m appeared to be a fundamental feature in the density distribution (Fig. 3c), forming a "density constriction" around density values of ~14-14.5 σ_t units. This depth is approximately the bottom of the upper layer subject to convective mixing. Above this depth, salinity showed a rather homogenous vertical profile with salinity values between 17.5 and 18.5 psu. We restate here that the Argo floats observe only the deep part of the Black Sea (coastal waters are not represented in Fig. 3); therefore, the homogeneity in salinity is explained as (1) a result of the intense circulation and mixing in the upper layers and (2) a consequence of the distribution of fresh waters from rivers over large shelf areas, thus diminishing the signature of the low-salinity source.

The almost-uniform salinity in the surface layer in the horizontal direction compared to the large spread of temperature and the almost-uniform temperature below the seasonal thermocline compared to the large spread of salinity explained the formation of the "density constriction" layer, which has very small density contrasts at ~40 m deep. In the overlying layers, the variability of temperature was large because of seasonal changes; in the underlying layers, salinity variations were large because of dynamics. This large spread of salinity profiles in the main halocline (between 50 and 250 m) represented the fact that the cyclonic circulation tended to displace the isohaline surfaces in the basin interior to shallower depths with respect to deeper depths along the coast (Stanev et al., 2000). This finding is illustrated in the bottom panels of Fig. 3, where the mean temperature, salinity and density for the whole period of observation are shown for the interior basin (depths larger than 1500 m, solid lines) and coastal ocean (depths less than 300 m, dashed lines). Intermediate depths (on the continental slope) are excluded in order to clarify the differences between the coastal and deep zone. Obviously, the vertical salinity profiles were more curved (sharper salinity stratification) in the basin interior, where upwelling brought saltier water closer to the surface. The opposite relation was observed in the coastal zone. The synthesis of the stratification in the upper ocean is consistent with previous data. However, we will show in the following that it can be only considered as a first-order explanation of the complex thermohaline processes. Thus, a deeper understanding needs to address diapycnic and isopycnic mixing in more detail.

Additional information about the temporal variability of stratification is given in Fig. 3 to facilitate the analyses in the following sections. Dotted, dashed and full lines in the upper panels show the mean vertical profiles during three almost equidistant two-year periods (2006 & 2007, 2012 & 2013, and 2017 & 2018). These periods were chosen such that they are representative for the beginning, middle and end of the observational time. The displacements of mean profiles from each other give a measure of the trends. Notably, temperature, salinity and density stratification decreased, which is inconsistent with the results of Yilmaz et al. (2006), who related the stronger stratification to ocean warming from 1995 to 2002. However, in the period addressed here, the stratification decreased. Obviously, further research is needed to increase the credibility of different analyses, which might be dependent on specific observational platforms. Keeping in mind possible problems with the quality of Argo data in the surface layer, our conclusions can be considered credible for depths below 15-20 m. However, a non-trivial question is whether recent climate change in the Black Sea tends to increase or decrease stratification and whether these changes are monotonous over long periods.

4. Temporal variability of water mass formation

4.1 Temporal evolution of the CIL

The warming of the CIL in recent decades has been documented in a number of studies (Stanev et al., 2013, 2014, 2017; Capet et al., 2016, Akpinar et al., 2017) that used data from profiling floats. On a shelf in the northern Black Sea, Mihailov et al. (2016) reported a warming of the upper mixed layer (~0.1 °C/year during 1971–2010) but not substantial changes of the cold water mass temperature. Below, we will revisit the temporal evolution of the CIL using all available data from profiling floats.

The time versus depth diagrams in Fig. 4 give a nontraditional presentation of the evolution of the oceanic thermohaline state based on all Black Sea Argo data. Each profile appears chronologically, which means that two neighboring profiles could originate from floats operating in different areas of the basin. One way to avoid such a “mix” among data from different areas would be to analyze data from each float separately. This approach was used by Stanev et al. (2013) and Akpinar et al. (2017) and is illustrated for all floats in Supporting Information, Fig. S3; however, the latter presentation is difficult to interpret. One alternative way to present the temporal variability is to average the data from all available locations for,

e.g., fortnightly periods. Such an alternative presentation would suffer from too few data used for averaging (from one to ~20). Another drawback would be that averaging would remove events seen by the individual floats.

The almost synchronous response of the upper 150 m layer to changes in atmospheric forcing is illustrated in Fig. 4 by the rhythmic change in vertical profiles of temperature and salinity. The temperature range in Fig. 4a and Fig. 4d is limited to only 7.5-8.9°C to show the details in the structure of the CIL. The continuous trend of increasing temperatures in the core of the CIL (Fig. 4a) appears to be the basic change in the cold water mass. Higher temperatures in the surface layers represented by the gray 20°C isoline in Fig. 4d show a quasi-periodic seasonal signal. The gray 8.7°C isoline is chosen to represent the approximate upper and lower boundaries of the CIL at present. This value is much larger than the "canonic" value of 8°C proposed by Blatov et al. (1984). With the 8°C boundaries, the CIL would currently appear as an outlier from the dominant stratification. The Argo floats registered water with temperatures lower than 8°C in the core of the CIL during only the first 3-4 years of the total observational period. To demonstrate the warming over a longer period, the mean basin temperature data at 50 m from the survey in July 1992 (Oguz et al., 1998) and from RV Akvanavt cruise 20 in the Eastern Black Sea (42,95°N, 39.11°E) in December 2000 are also shown in Fig. 3a, For the respective Akvanaft profiles, see Fig. 2 from Stanev et al. (2014). During the first survey, the coldest temperature of the CIL was ~7°C; whereas during the second survey eight years later, it was ~7.5°C. The above comparison with the historical data shows that in the last 2-3 decades, the temperature in the core of the CIL has increased by more than 1°C.

The question then arises about the highest temperatures above which the CIL will disappear. Fig. 3a gives the answer and shows that the temperature at intermediate depths is now ~9°C (see the vertical line). The CIL cannot be warmer than this value, and it will disappear as a basin-wide thermal characteristic unless the temperature of deep and intermediate water increases (e.g., by warmer inflow from the Marmara Sea). Obviously, the CIL currently presented as a layer bounded by the 8.7°C isotherms is close to a state of disappearance (~9°C).

We do not show the 8.7°C boundaries in Fig. 4a because of the "noise" associated with the fact that two consequent observations could originate from areas with different dynamics. The

amplitude of this “noise”, which actually gives a measure of the variability of the depths of isopycnic surfaces, is ~25 m. When many floats are operating at the same time, this isoline, if plotted as in Fig. 4d, looks like a thick gray band because of the large amount of data measured in a short time in different areas. This finding is consistent with earlier analyses of profiling floats in the Black Sea (Stanev et al., 2013; 2014), and it is explained by the large differences between vertical profiles in the areas occupied by cyclones and anticyclones. Therefore, significant differences between the CIL characteristics occur (Akpinar et al., 2018), particularly if the data are presented in depth coordinates.

To avoid masking the underlying colors, we do not show the 8.7°C isotherm in Fig. 4a. The upward displacement trend of the bottom of the CIL of ~50-70 m for the whole period of observations is much larger than the amplitude of ~25 m associated with the different depths of the 8.7°C isotherm in the zones of upwelling and downwelling. This result clarifies that the warming of the CIL in the last decades was far stronger than the “noise” due to using the specific observational and analysis platform.

Presenting the data in density coordinates (panels at the bottom of Fig. 4) reduces the scatter of data shown in Fig. 4a, thus decreasing the effects of regional differences seen when presenting the same data in depth coordinates. Therefore, the following analyses allow us to draw conclusions about the basin-wide changes in the thermohaline state of the Black Sea. Applying this approach (data from different areas shown in chronological order) for larger open ocean areas is not straightforward and has to be preceded by a careful examination of the regional conditions.

The disappearance of the low-density values in the bottom panels of Fig. 4 during the cold part of the year is explained by the colder temperatures resulting in high density. Notably, the time versus density diagram is not a full matrix of valid data because low-density values do not exist in winter. The water mass formation events appeared during the outcropping phase between two consecutive seasonal peaks.

The reduction of the cold water content in the CIL was manifested not only by the warming of its core but also by the displacement of its boundaries. The representation in density coordinates clearly reveals that the last 14-year period was characterized by only three major cold water formation events; each event was much weaker than the previous one. One very important finding, which was possible because of the continuous observations and the

availability of measurements in different areas, was the "perforation" of the CIL, which means that at specific periods and locations, the CIL disappeared (the 8.7°C isoline extended from the surface layers down to ~200 m). This effect is seen in the "chimney-like" local events, which occurred during 2015-2017, i.e., the periods when the CIL almost disappeared basin-wide.

The salinity stratification depicts a two-layer structure with less salty water in the surface layer (Fig. 4b). Unlike the temperature profiles, the salinity profiles are monotonic; i.e., salinity always increased with depth. The oscillations observed in geometric coordinates, which are mostly due to the spatial variability of salinity, decrease strongly when salinity evolution is presented in density coordinates (Fig. 4e). Obviously, this type of presentation is more appropriate for addressing the synchronous thermohaline changes over the entire basin. Below 100 m, the density pattern almost repeats the salinity pattern (not shown here), demonstrating that the temperature at these depths does not have a pronounced dynamic effect. Further details about the inter-relationship between thermohaline characteristics are given in section 5.

Compared with many earlier studies that analyzed the dynamics of the CIL in the Black Sea by examining the temperature changes only (one exception is the work of Piotukh et al. (2011), which analyzes both temperature and salinity in the northeastern Black Sea), we emphasize the analysis of salinity. The latter provides the dominant contribution to the density stratification in the intermediate and deep layers. This stratification in the Black Sea is so strong that sometimes its changes are not easy to identify. Therefore, in Fig. 4c and Fig. 4f, we show the temporal variability of the salinity anomaly (the mean of the vertical salinity profile for the whole period is subtracted from the current profiles). The magnitude of salinity change shows a maximum at ~80 m that is at the upper boundary of the halocline (Fig. 4b). This depth is approximately where the pycnocline shows the largest slope. Unlike salinity, the magnitude of temperature change was maximum at the surface. The magnitude of the variabilities of the two thermohaline characteristics change so that at ~80 m (between the core of the CIL and its lower boundary), the thermal and haline *changes* almost compensate in the density field. This situation reflects the known compensation of temperature and salinity effects along many ocean fronts (Rudnick and Ferrari, 1999) and directs the following discussion of a comparative analysis of temperature and salinity changes.

The salinity anomaly trends, as seen in geometric coordinates, revealed two periods: one period, before 2012, was characterized by intermittent changes in the salinity anomaly, and the other period, after 2012, had a rather rhythmic occurrence of positive salinity anomalies along the axis of the CIL (Fig. 4c). The amplitudes were larger in the second period. Minima occurred in the summer, and a relatively wide maximum dominated the rest of the year. The presentation of the salinity anomaly in density coordinates (Fig. 4f) clearly illustrates the vertical propagation (diapycnic mixing), which in recent years appeared as positive salinity-anomaly signals crossing layers between σ 15 and 17 and propagating below the axis of the CIL (compare Fig. 4f with Fig. 4d).

The event at the beginning of 2010 (strong negative anomaly in Fig. 4c) needs specific attention. For approximately three months, float 1901200 operated along the southern coast. On January 30 and February 4, it collected profiles in the area east of the Sakarya Canyon (see the large triangle symbols in Fig. 1 for its two positions). During this time, the strongest cooling for the total period analyzed here was observed (Fig. 2). The float was close to the coast where salinity was rather low because of the runoff from the Sakarya River. The extreme cooling and the low salinity, in combination, resulted in the low-temperature and low-salinity anomaly penetrating more than 200 m deep (Fig. 4 b, c). This process also explains the maximum negative salinity anomaly seen in Fig. 4c.

4.2 Replenishment of the CIL with cold water and mixing with surface and deeper waters

To the best of the authors' knowledge, no estimates of the dominant time scales associated with refill events are available based on long-term analyses or analyses of refill occurrence at the interannual time scales. Argo floats provided a perfect opportunity to fill this gap. In the following, we provide a different view of the evolution of the CIL, complementing the analysis of Fig. 4 and focusing on the seasonality, the short-term intermittency, and the interannual changes. Fig. 5 presents the temporal variability of temperature, salinity and density at 25, 50 and 100 m. Each of these depths yields representative information on the evolution of the surface layer and the upper and lower parts of the CIL. Although these fixed depths along the trajectory cannot be generalized to the whole basin, the analysis below is instructive for the overall evolution of upper-ocean thermohaline fields.

The surface layer (25 m) shows rather periodic variability. Parts of the period before 2010, namely, 2005-2006, were sampled by two floats only (see the inset in Fig. 1 and the Supporting Information); therefore, the density of data was low. The temperature at this level decreased to less than 6°C only three-four times, a value close to the lowest monthly mean air temperature from atmospheric analyses (Fig. 2a). These cooling events appeared well in phase with the extremely low atmospheric temperatures at the Varna station in Fig. 2. The warming trend at 25 m was revealed by the continuous increase in the maximum temperatures, particularly after 2012, when they were higher than 25°C. This trend was much better pronounced than that seen in the summer atmospheric temperatures in Fig. 2a, which could suggest other causes, such as variations in the mixed layer depth. One such example is the case observed by float 4900540 in 2005, when the maximum temperature at 25 m was only ~10°C. The detailed analysis of the data recorded by this float showed that the low temperature at 25 m was due to the very shallow seasonal thermocline.

Not every cooling event in the upper layers reached the core of the CIL, particularly during the mild winters (compare temperatures at 25 and 50 m in Fig. 5a and Fig. 5d). The sensitivity of water mass formation to the magnitude of surface cooling was proven by the fact that with slightly warmer minimum temperatures at 25 m (e.g., ~1.5°C higher compared to the coldest winters), the signature of cold water mass formation at 50 m was cancelled. Only three cooling events were observed at 50 m with temperatures as low as ~6.5°C. Atypically high temperatures for the CIL occurred in some of the summer profiles (up to 16°C), especially during the second half of the analyzed period, which is explained by the fact that the depth of 50 m is still too close to the sea surface. The long-term temperature trend at 50 m was also quite pronounced. While the temperatures during the first half of the observational period were usually less than 8°C, during the second half, they were lower than this value only during the periods of the major cooling events in 2012 and 2017. Notably, during 2012-2016, cold water formation did not occur for several years. Because of this situation, the lowest temperatures at 50 m increased slowly after 2012, with an exponential rate of approximately 4-5 years, which compares well with the earlier estimates of the ventilation times (Ovchinnikov, 1998; Lee et al. 2002; Stanev et al., 2003).

The warming phases observed in the periodic summer maxima at 50 m originating from the surface layers disappeared at 100 m, with the exception of several individual events after 2014. These events did not occur synchronously with the warming at 50 m but rather

coincided in time with several major intrusions of Mediterranean water reported by Stanev et al. (2017). Obviously, the layer at 100 m encapsulated the major signal of the interannual and long-term variability of the CIL (Fig. 5g). The interannual variability was represented by the three cooling events, which appeared rather abruptly and faded slowly over time. The long-term trend was represented by the continuous increase in maximum temperatures at this depth.

The fact that the variability of density at 25 m almost mirrors that of temperature (compare Fig. 5a and Fig. 5c) demonstrates that in the surface layer, the surface salinity acted as a passive tracer. While the seasonal variability of salinity in the surface layer was not well pronounced (Fig. 5e), the salinity trend over the last fourteen years was clear (see also the displacement of profiles to the right in Fig. 3b). The continuous increase in salinity would suggest that, during this period, the fresh water flux decreased. However, the analysis of total precipitation over the Black Sea from ERA-5 data did not show a decreasing trend. One possible explanation is given below.

4.3 Relationship between temperature and salinity

The basic hypothesis of the present research is that the evolution of CIL cannot be fully described by the evolution of temperature only. The questions then are as follows: (1) what is the role of salinity and (2) what is the relationship between temperature and salinity. Temperature and salinity are conservative fields under the assumption that the light absorption and ecosystem processes, which could affect temperature, are not considered. Then, both fields are subject to surface sources, Bosporus Strait sources and geothermal fluxes (see the introduction). Their joint effect on density gradients can either enhance or compensate depending on the distribution of sources and specific dynamics, which can be identified by analyzing their correlation.

For the total period of observations, the correlation between temperature and salinity at 25 m was low at ~ -0.30. The negative sign (low temperature in winter was accompanied by high salinity) would indicate that the convective mixing brought higher salinity water from beneath into the surface layer. This implication is contrary to the scenario assuming that winter cooling would bring colder and less saline water from the surface into the deeper layers. One exceptional case was observed in 2010 by float 1901200 in the proximity of the Sakarya River. The dominance of the first scenario would imply that the homogenous salinity in the surface layer (Fig. 3b) provided too weak a fresh water source compared to the strongly

stratified layers beneath. Thus, the decreasing salinity stratification shown in Fig. 3b in the last fourteen years (that is, the increase in salinity in the surface layers) had as a source the high-salinity pool in the intermediate and deep layers.

The correlation between temperature and salinity at 50 m (-0.26) was even slightly weaker than that in the layers above, and the salinity evolution was very irregular (Fig. 5e). This irregular salinity variability appears because Fig. 5e presents mixed data from different floats operating in different areas of the sea. Unlike the case at 25 m, the density variability at 50 m did not repeat the temperature variability or the salinity variability. This result suggested that the salinity effect on buoyancy at 50 m became comparable to that of temperature. The positive trend for the entire period was comparable to that at 25 m.

With increasing depth, the correlation between temperature and salinity reversed sign at ~70 m, increasing to 0.49 at 100 m and 0.74 at 250, remaining high down to 300 m . This depth interval is where the maximum seasonal amplitudes of salinity anomalies were observed. The positive correlation indicates that the changes in the thermohaline state of this layer were mostly impacted by mixing with the waters from above (low temperature in the CIL and low salinity in the upper layers). The temperature in the layers below was very homogeneous, and the density plots (not shown here) almost repeat the salinity plots.

The weak temperature signature in the deeper layers would suggest that the thermohaline characteristics of mixed water at 100 m were less affected by mixing with the underlying water and more affected by mixing with waters from the core of the CIL. Furthermore, between 100 and 250 m, the pycnocline showed the largest slope, and this slope was greatest in the area of the rim current. Therefore, the strong correlation between temperature and salinity plausibly reflects the mixing in the front-area, separating warmer and saltier water in the interior basin from cooler and less salty waters in the coastal area. This result shows that dynamics could play a major role in controlling water mass formation in the Black Sea and supports the modeling study of Stanev and Staneva (2001) and the observations of Ostrovskii and Zatsepin (2016), who demonstrated that the appearance of ventilation events depends on the intensity of the rim current.

A better understanding of the changes in the second half of the observational period is provided by Fig. 5i, showing the difference between the product of temperature and salinity

from which we subtracted the mean for each layer product of temperature and salinity over the total period of observations: T×S–<T×S>. Here, <.> is a function of depth. During the first phase, the positive variance of temperature and salinity was rather shallow and weak, and the negative variance was well pronounced; a reversal occurred during the second phase of the observational period. After 2012, an intermediate layer with positive T×S anomaly was observed at the depths of the CIL. Obviously, the long-term evolution of the CIL is a process of joint evolution of temperature and salinity.

5. Dynamic T-S analysis

The following discussion addresses the interrelationship between the thermohaline states of the Black Sea represented by the position of a current T-S pair in the space of temperature and salinity ranges. The T-S relationship (Fig. 6a) showed a rather scattered distribution of T-S indices, particularly in the surface layer, subject to strong seasonal variability. The color coding represents the time of observations. Plotting this large amount of data in one scatterplot would result in overlapping symbols. Because the number of observations per year during the earlier phases of the Argo program was lower, we plotted the data in an inverse time order ("sparse" old data overlie more recent measurements). Even with such a caveat, the figure illustrates nicely that the T-S characteristics changed substantially during the observational period. Water with a temperature of 10°C became saltier, and water with a salinity of 19 became warmer in recent years.

The temperature-density relationship was almost linear throughout the depth range where the temperature was higher than 10°C, approximately following isohaline 18 (Fig. 6b). This result illustrated that in the surface layer, temperature provided the basic contribution to density. This almost linear relationship was a representation of the conservative mixing between two endmembers: warm surface water and water from the CIL. Below the CIL, linear mixing dominated the salinity-density relationship (Fig. 6c). The "density constriction" at σ_t~14.25 (section 3.1) is where the transition between two regimes occurs. In other words, the CIW is "in the corner" in the T-S diagram, where the plots make a curve at ~18 salinity and ~9°C.

The changes in the T-S relationship of individual profiles in Fig. 6a indicated that a fundamental change in the mixing processes between the surface and deep layers occurred recently in the CIL. This shift can be inferred from the different curvature of profiles (Stanev et al., 2014), indicating that the recent alterations in the thermohaline state of the Black Sea

542 are associated with changes in the vertical (diapycnic) mixing in the core of the CIL (see also
543 Fig. 4d).
544
545 The full presentation of the change of the thermohaline state would necessitate considering it
546 in the 4D space defined by temperature, salinity, pressure and time. For the observational
547 platform used here, the time carries information on the positions of the individual profiles.
548 Displaying the thermohaline state in 4D is challenging, partially because of the very large
549 amount of data; therefore, we present below three subspaces of data for three individual σ_t
550 depths: 14.5, 15 and 15.5 (see the respective isolines in Fig. 6a). If we replot Fig. 6a for these
551 individual σ_t depths separately and ignore all data that are not on these surfaces, then the T-S
552 pairs would overlap on the respective density line because some individual states (observed at
553 different times and locations) could have the same T-S characteristics. Similar to the result in
554 Fig. 6a, the overlapping would "hide" the temporal evolution described by the movement of
555 T-S indices on the respective σ_t surface.
556
557 The subspace of Fig. 6a at three density levels would look like scatterplots along three -σ_t
558 lines. To present an appropriate temperature-salinity resolution in the separate T-S plots, one
559 can select appropriate T-S ranges (e.g., different from the ones in Fig. 6a), which results in a
560 slope change for the respective density line (see as an example the sloped dotted lines in Fig.
561 7).
562
563 An analysis of the response of the Black Sea to regional climate variations (warming) can
564 justify keeping the temperature as the dominant axis (y-axis in Fig. 7). Then, we have only
565 one additional dimension left in 2D space for time, salinity and pressure. The slopes of the
566 dotted lines in Fig. 7 correspond to the T-S ranges given in the caption of Fig. 7. These
567 different slopes reveal the relative contribution of temperature and salinity to the buoyancy
568 and approximately reflect the density ratio $R = \alpha\, \Delta T/\beta \Delta S$, where $\alpha = 1.3\times10^{-4}$°C^{-1} and $\beta =$
569 7.5×10^{-4} psu^{-1} are the coefficients of temperature expansion and salinity contraction,
570 respectively (we actually used the full equation of state). Each individual observation at the
571 specified σ_t level is presented in Fig. 7 in the respective T-S range. However, the salinity of
572 every next observation is shifted in time to the right by a prescribed value, which is
573 proportional to the elapsed time between observations. In this way, we "unfold" the changes
574 in T-S indices in time. Thus, the x-axis must be understood as a modified time coordinate
575 (salinity is implicitly included by the slope of density curves). The density line is repeated

every second year to illustrate the phase of events with respect to the times shown on the x-axis. The remaining variable, the pressure, is shown by colors.

The individual panels in Fig. 7 correspond approximately to the temperature and salinity variations for several individual depths (Fig. 5d, e, g, h). However, the thermohaline evolution at specific σ_t levels (Fig. 7) shows smaller scatter than in Fig. 5. The overall increase in temperature was common to all density levels in the CIL. This increase was "interrupted" by individual events of cooling from the surface and warming due to the intrusions of Marmara Sea waters. This representation in density coordinates shows the evolution of mixing characteristics. The cold water mass formation is well represented as short-lived oscillations aligned along the density lines. These maximum deviations from the mean long-term evolution of the thermohaline state reveal the endmembers subject to isopycnic mixing. These almost linear mixing curves connect two endmembers: young CIW and old CIW. The latter is found in deeper layers. The isopycnic surfaces of the new CIW are shifted to lower pressure levels (blue color in Fig. 7a) during the water mass formation events.

The individual cooling events were separated by relatively long periods of slow increases in temperature and salinity at σ_t = 15 (Fig. 7b). During this phase, the trajectories of T-S indices were crossing isopycnic lines, suggesting that the evolution of the T-S pairs illustrated diapycnic mixing. As observed in the period 2014-2015, mixing with deeper layers (warmer temperatures) occurred at higher pressures (symbols plotted with red color). The mixing curves at σ_t = 15 during the major cold water formation events were also almost straight lines connecting the two endmembers: the young CIW (very shallow) and the old CIW, the latter found in deeper layers. Minor cold water formation events were almost not observed at this density level. In contrast to that in the upper density layer, the scatter of data at σ_t = 15 was smaller, and there were very clear trends of continuous increases in temperature and salinity that were interrupted by perturbations associated with water mass formation.

The evolution of the thermohaline state at σ_t = 15.5, which is approximately at the bottom of the CIL, shows less pronounced short-term variability and clearer long-term trends, suggesting that convection did not efficiently reach these depths (Fig. 7c). The short-term changes were instead associated with warm intrusions of Marmara Sea waters at deeper levels (red colors). The longer time needed for the cooling phase during 2012 at this level than at σ_t = 15 reflected the diffusive penetration of cooling from above. In the warming phase, the

high-pressure profiles were those with higher temperatures, reflecting warming from below and cooling from above. The cooling event that started in 2012 show a number of profiles for which the colder water was observed at deeper pressure. Fig. 4d facilitates the explanation, illustrating that this cooling event resulted in an overshoot of deep convection and the availability of cold water in the deep ocean. Approximately one year was needed for the high-temperature profiles to move to greater depths.

6. Discussion

This study provides diagnostics of the change in the Black Sea thermohaline state during the last 14 years. Obviously, not only the upper layer but also the Black Sea pycnocline responds to climate change. Of particular importance were the observed changes in salinity (Fig. 4c, 4f) occurring at the same depth and density ranges where the CIL is usually observed. Therefore, the CIL is not just a temperature signature, as it was considered in some earlier studies; it is a layer where the strong correlation between temperature and salinity gives a measure of their collective role in the evolution of the Black Sea dynamics.

In the Black Sea, the slope of the pycnocline gives the best (integrative) measure of the basin-scale dynamics. One could expect that the changes in stratification, specifically, the structure of the water masses, could also have affected the Black Sea circulation. This interpretation would sound speculative because the opposite hypothesis is also possible; that is, changing the wind regime could have affected the circulation. This change would affect the exchange across the density surfaces and, finally, the structure of water masses. Furthermore, as shown on the example of float 4900540 in 2005 (very low temperature at 25 m explained by very shallow seasonal thermocline), the wind effects setting up the depth of the mixed layer need further consideration when analyzing the dynamics of water mass formation and transformation. The analysis of data only cannot easily identify the causality and the contributions of individual mechanisms that led to the recent change. This dilemma presents a challenge for dedicated numerical studies.

The individual contributions of external drivers, such as changes in winds, river runoff, and exchange in the Bosporus Strait, must also be evaluated. Some of these constituents of the external forcing are not independent. As demonstrated by the observations of Jarosz et al. (2011) and the numerical simulations of Stanev et al. (2017), wind over the Bosporus Strait could either block the inflow or increase it by a factor of three compared to the mean value.

This large variability explains the variety of intrusions at intermediate and deep levels (Stanev et al., 2017; Falina et al., 2017). Coupled dynamics of the CIL and intermediate layers could plausibly be of utmost importance for the future states of the Black Sea. Here, the use of dedicated numerical studies seems mandatory.

From the presented results, the long-term evolution of the CIL seems evidently a process involving the joint evolution of temperature and salinity. This evolution is associated with the dynamics of the frontal zone (rim current) and its mixing. One further challenge would be to understand the individual or collective trends of thermohaline states in the coastal ocean and deep ocean. Unfortunately, the Argo platform (observations in the deep ocean only) cannot fully address the role of the coastal ocean; thus, the contribution of coastal oceans to the overall thermohaline state needs more attention (Shapiro et al., 2011; Mihailov et al, 2016). This type of study is necessary because the most important components of water balance, i.e., rivers and exchange with the Strait of Bosporus (the major haline-driving factors), are in the coastal ocean.

The present trends, if they remain at their current levels, suggest that the 8.7°C isotherms used in Fig. 4 to specify the position of CIL would cross after approximately 15-20 years (see Fig. 4a and 4d). However, as better shown in Fig. 4d, the steepness of the trends increases; therefore, one could expect that the CIL would disappear even sooner. One could expect that, in the future, the coupled variability of temperature and salinity will become stronger, as suggested by the trend in Fig. 5i. Another speculation about the further development of the CIL is that the contribution of the northwest shelf, where the temperatures are still low, to the formation of cold water will increase relative to the contribution from the open ocean and southern coastal regions.

The Black Sea case is one among many other similar cases of rapid changes. Kniebusch et al. (2019) compared the time periods 1856-2005 and 1978-2007 and revealed that the SST trends in the Baltic Sea strengthened by 10-fold. In the Mediterranean, an abrupt shift in the structure of deep and abyssal water masses occurred in the 1990s (Roether et al. 2007). It seems obvious that the clear signals of change in the water masses in semi-enclosed and other regional basins can be considered amplified precursors of the changes to expect in the greater oceans.

7. Conclusions

The Black Sea represents a perfect ocean area to study the disappearance of certain water masses caused by climate change. The detection of substantial changes in the structure of water masses became feasible in the era of Argo floats, as demonstrated in the present study on the example of the evolution of the CIL. Observations showed that the temperatures in the CIL are currently substantially higher than the values known from historical data. Temperatures lower than 8°C, which was used in the past to specify the upper and lower boundaries of the CIL, are presently outliers. The Argo floats registered temperatures in the core of the CIL lower than 8°C during only the first 3-4 years of the last 14 years. Starting in 1991, the temperature in the core of the CIL increased by more than 1°C until now, which was mainly due to an increase over the last fourteen years of 0.7°C degrees. The comparison between the atmospheric and oceanic data demonstrated that the ocean trends were largely explained by the warm winters, more specifically by the absence of extremely low temperatures and cold events that persisted for long periods. These changes reflected the increase in the lowest monthly mean winter air temperatures during the last 14 years. As a response to the warming signal in the atmosphere, the cold water mass formation in the Black Sea became rather intermittent, and amplitudes decreased. The cold water content in the CIL reduced and its lower boundary displaced upwards. Presently, the temperatures of the CIL approach ~ 9°C; thus, this layer tends towards a state of disappearance.

Of particular importance was to identify the sources of water masses and mixing between the cold waters and waters below and above the CIL. In the upper layer, the major variability in the open sea was due to temperature; salinity in this layer was rather uniform. Below the CIL, salinity showed the major contribution to the density variations. At ~40 m, a narrow "density constriction" around density values of ~14-14.5 reflected a layer with minimum change in density. These values marked the density interval where the CIW penetrated the halocline (Stanev et al., 2003). At these depths, the effect of salinity in the density field starts to compete with the effect of temperature. Between the core of the CIL and its lower boundary, the thermal and haline changes almost compensate. The correlation between temperature and salinity at 250 m is at a maximum, thus reflecting the mixing in the area of rim current. This current separates warmer and saltier water in the interior basin from cooler and less salty waters in the coastal area, and changes in its intensity control the strength of ventilation.

The interrelationship between salinity and temperature is an important indicator of changes in Black Sea water masses. The trajectories of T-S indices in the space defined by temperature, salinity and time were addressed by unfolding in time the T-S relationships at given σ_t levels. This analysis appeared to be a useful tool to detect the basic changes in the thermohaline structure and to illustrate the mixing between waters of different origin (endmembers). The basic trend in the CIL revealed by the diagrams in Fig. 7 demonstrated a drift from the bottom left to the top right. This increase in both T and S was due to diapycnic mixing, which was manifested by the fact that the trend line crossed the σ_t surfaces. The unfolded presentation in Fig. 7 clearly illustrates the individual cooling events as well as the contribution of levels at different depths to the formation of the CIL. These events were very pronounced in the vicinity of the “density constriction” (Fig. 7a), i.e., “in the corner" in the T-S diagram where the individual profiles in Fig. 6a make a curve at ~18 salinity and ~9°C.

Two thermohaline regimes were identified: one period before 2010, when the salinity anomaly in the CIL showed rather intermittent low-amplitude changes, and the other period after 2010, when the salinity anomaly occurred in a rhythmic way. During the second period, shown Fig. 4c and f, the amplitude of salinity variability increased, and a pronounced propagation of the salinity anomaly signal was clearly observed down to the bottom of the CIL.

Acknowledgments. The authors thank P. M. Poulain and V. Slabakova for the deployment and technical maintenance of certain floats. We are grateful to the three anonymous reviewers for their constructive comments. Data used in this study are available at: ftp://ftp.ifremer.fr/ifremer/argo/dac/coriolis/, http://marine.copernicus.eu/, https://www.ogimet.com/, and https://climate.copernicus.eu/. This study was supported by the EU-funded project Black Sea – Monitoring Forecasting Centre (BS MFC) in the frame of the COPERNICUS Marine Environment Monitoring Service (CMEMS).

738 **References**

739 Akpinar, A., Fach, B. A. & Oguz, T. (2017): Observing the subsurface thermal signature of
740 the Black Sea cold intermediate layer with Argo profiling floats. *Deep Sea Research Part I:*
741 *Oceanographic Research Papers*, **124,** 140-152, http://dx.doi.org/10.1016/j.dsr.2017.04.002
742 ARGO (2000) Argo floats data and metadata from Global Data Assembly Centre (Argo
743 GDAC), Tech. rep., Ifremer
744 Argo data management (2013) Argo users manual, Tech. rep., Ifremer. doi:10.13155/26387
745 Blatov, A. S., Bulgakov, N. P., Ivanov, V. A., Kosarev, A. N., & Tujilkin, V. S.
746 (1984)Variability of Hydrophysical Fields in the Black Sea, Gidrometeoizdat, Leningrad, 240
747 pp. (in Russian).
748 Capet, A., Stanev, E. V., Beckers, J.-M., Murray, J., & Gregoire, M. (2016). Decline of the
749 Black Sea oxygen inventory. Biogeosciences, 13(4), 1287–1297. https://doi.org/10.5194/bg-
750 13-1287-2016
751 Capet, A., Troupin, C., Carstensen, J., Grégoire, M., & Beckers, J.M. (2014): Untangling
752 spatial and temporal trends in the variability of the Black Sea Cold Intermediate Layer and
753 mixed Layer Depth using the DIVA detrending procedure Ocean Dynamics 64 (3), 315-324
754 Falina, A., Sarafanov, A., Ozsoy, E., & Turuncoglu, U. U. (2017). Observed basin-wide
755 propagation of Mediterranean water in the Black Sea. J. Geophys. Res. Oceans, 122,
756 doi:10.1002/2017JC012729
757 Grayek, S., Stanev, E.V. & Schulz-Stellenfleth, J. (2015): Assessment of the Black Sea
758 observing system. A focus on 2005-2012 Argo campaigns. Ocean Dynamics 65: 1665.
759 https://doi.org/10.1007/s10236-015-0889-8
760 Gregg, M. C. & Yakushev, E. (2005). Surface ventilation of the Black Sea's cold intermediate
761 layer in the middle of the western gyre. Geophys. Res. Lett., 32, L03604,
762 doi:10.1029/2004GL021580
763 Jarosz, E., Teague, W. J., Book, J. W., & Besiktepe S. (2011). Observed volume fluxes in the
764 Bosphorus Strait. Geophys. Res. Lett., 38, L21608, doi:10.1029/2011GL049557.
765 Kniebusch, M., Meier, H. E. M., Neumann, T., & Börgel, F. (2019): Temperature variability
766 of the Baltic Sea since 1850 and attribution to atmospheric forcing variables. J. Geoph. Res.,
767 https://doi.org/10.1029/2018JC013948
768 Kolesnikov, N. (1953). Seasonal course of temperature, stability and vertical turbulent heat
769 exchange in the open part of the Black Sea. Trudi Mor. Gidrol. Inst. USSR AS, 3, 3–13.
770 Konovalov, S. K., Murray, J. W., & Luther, G. W. III. (2005). Basic processes of Black Sea
771 biogeochemistry. Oceanography, 18, 24-35.

772 Korotaev, G. K., Knysh V. V., and Kubryakov, A. I. (2014). Study of formation process of
773 cold intermediate layer based on reanalysis of Black Sea hydrophysical fields for 1971–1993.
774 Izvestiya AN. Fizika Atmosfery i Okeana, 50 (1), 35-48.
775 Korotaev, G., Oguz, T., & Riser, S. (2006). Intermediate and deep currents of the Black Sea
776 obtained from autonomous profiling floats. Deep Sea Res. Pt II 53, 1901–1910
777 Lee, B. S., Bullister, J. L., Murray, J. W. & Sonnerup, R. E. (2002). Anthropogenic
778 chlorofluorcarbons in the Black Sea and the Sea of Marmara. Deep-Sea Res. I, 49, 895–913.
779 Mihailov, M.–E., Stefan, S., Diakonu, V., & Lazar, L. (2016): Longterm variability of the
780 water mass structure on the Romanian Black Sea Shelf. *Romanian Reports in Physics, **68**, 1,*
781 *377–392.*
782 Miladinova, S., Stips, A., Garcia-Gorriz, E., & Macias Moy D. (2017). Black Sea
783 thermohaline properties: Long-term trends and variations. J. Geophys. Res. Oceans, 122,
784 5624–5644, doi:10.1002/2016JC012644.
785 Oguz, T., Ivanov, L.I. & Besiktepe, S. (1998): *Circulation and hydrographic characteristics*
786 *of the Black Sea during July 1992*. In: L. Ivanov and T. Oguz, eds, Ecosystem Modeling as a
787 Management Tool for the Black Sea, NATO ASI Series, Environmental Security - vols. 47, 2.
788 Kluwer, Dordrecht, pp. 69-92.
789 Oguz, T. & Besiktepe, S. (1999): Observations on the Rim Current structure, CIW formation
790 and transport in the western Black Sea. Deep Sea Research Part I: Oceanographic Research
791 Papers 46 (10), 1733-1753.
792 Oguz, T., Dippner, J. W., & Kaymaz, Z. (2006). Climatic regulation of the Black Sea hydro-
793 meteorological and ecological properties at interannual-to-decadal time scales, J. Marine
794 Syst., 60, 235–254, doi:10.1016/j.jmarsys.2005.11.011, 2006.
795 Ostrovskii, A. G., & Zatsepin, A. G. (2016). Intense ventilation of the Black Sea pycnocline
796 due to vertical turbulent exchange in the Rim Current area. Deep-Sea Res. I 116, 1–13.
797 http://dx.doi.org/10.1016/j.dsr.2016.07.011.
798 Ovchinnikov, I. M. (1998). Interaction between surface and deep waters in the process of
799 transverse circulation of the Black Sea, in Ventilation of Black Sea Anoxic Waters. Workshop
800 Rep. Ser. 1/05/98, Liege, 135–161.
801 Ovchinnikov, I. M. & Popov, Yu. I. (1987). Evolution of the Cold Intermediate Layer in the
802 Black Sea, Oceanology, 27, 555–560
803 Ozsoy, E., & Unluata, U. (1997). Oceanography of the Black Sea: a review of some recent
804 results. Earth-Science Reviews 42, 231-272

Piotukh, V. B., Zatsepin, A. G., Kazmin, A. S., & Yakubenko, V. G. (2011). Impact of the winter cooling on the variability of the thermohaline characteristics of the active layer in the Black Sea. Oceanology 51 (2), 221–230. https://doi.org/10.1134/S0001437011020123

Roether, W., Klein, B., Manca, B. B., Theocharis, A., & Kioroglou, S. (2007). Transient Eastern Mediterranean deep waters in response to the massive dense-water output of the Aegean Sea in the 1990s. Progress in Oceanography, 74, 540–571

Rudnick, D. L., & Ferrari, R. (1999). Compensation of horizontal temperature and salinity gradients in the ocean mixed layer. Science, 283, 526-529.

Schott, F., Visbeck, M., Send, U., Fischer, J., Stramma, L. & Desaubies, Y. (1996). Observations of deep convection in the Gulf of Lions, northern Mediterranean, during the Winter of 1991–92. *J. Phys. Ocean.*, 26, 505–524

Shapiro, G. I., Stanichny, S. V., & Stanychna, R. R. (2010). Anatomy of shelf-deep sea exchanges by a mesoscale eddy in the North West Black Sea as derived from remotely sensed data, Remote Sens. Environ., 114, 867–875

Shapiro, G. I., Wobus, F., & Aleynik, D. L. (2011). Seasonal and inter-annual temperature variability in the bottom waters over the western Black Sea shelf. Ocean Sci., 7, 585–596, doi:10.5194/os-7-585-2011

Schrum, C., J. Staneva, E. Stanev, and E. Özsoy (2001) Air-sea exchange in the Black Sea estimated from atmospheric analysis for the period 1979-1993. *J. Mar. Sys.*, 31, 3-19.

Stanev, E. V., Bowman, M. J., Peneva, E. L., & Staneva, J. V. (2003). Control of Black Sea intermediate water mass formation by dynamics and topography: comparison of numerical simulations, surveys and satellite data. J. Mar. Res., 61, 59–99

Stanev, E., Grashorn, S., & Zhang, Y.J. (2017). Cascading ocean basins: numerical simulations of the circulation and interbasin exchange in the Azov-Black-Marmara-Mediterranean Seas system, Ocean Dynamics, 67(8), 1003–1025.

Stanev, E. V., He, Y., Grayek, S., & Boetius, A. (2013). Oxygen dynamics in the Black Sea as seen by Argo profiling floats. Geophys. Res. Lett., 40, 3085–3090, doi:10.1002/grl.50606

Stanev, E. V., He, Y., Staneva, J., & Yakushev, E. (2014). Mixing in the Black Sea detected from the temporal and spatial variability of oxygen and sulfide—Argo float observations and numerical modelling. Biogeosciences, 11(20), 5707–5732. https://doi.org/10.5194/bg-11-5707-2014

Stanev, E. V., Grayek, S., Claustre, H., Schmechtig, C., & Poteau, A. (2017). Water intrusions and particle signatures in the Black Sea: A biogeochemical-Argo float investigation. Ocean Dynamics, 67(9), 1119–1136. https://doi.org/10.1007/s10236-017-1077-9

839 Stanev, E. V., & Staneva, J. V. (2001). The sensitivity of the heat exchange at ocean surface
840 to meso and sub-basin scale eddies. Model study for the Black Sea. Dyn. Atmos. and Oceans,
841 33, 163–189.
842 Stanev, E. V., Le Traon, P.-Y., & Peneva, E. L. (2000). Seasonal and interannual variations of
843 sea level and their dependency on meteorological and hydrological forcing. Analysis of
844 altimeter and surface data for the Black Sea. J. Geoph. Res., 105, 17203-17216.
845 Staneva, J.V. Stanev, E.V., 1998. Oceanic response to atmospheric forcing derived from
846 different climatic data sets. Intercomparison study for the Black Sea. Oceanol. Acta 21, 393–
847 417.
848 Staneva, J. V., & Stanev, E. V. (2002). Water mass formation in the Black Sea during 1991–
849 1995. J. Mar. Sys., 32, 199–218.
850 Wong, A., Keeley, R., Carval, T. & the Argo Data Management Team (2019). Argo Quality
851 Control Manual for CTD and Trajectory Data. http://dx.doi.org/10.13155/33951
852 Yilmaz, A., Coban-Yildiz, Y., Telli-Karakoc, F., & Bologa, A. (2006). Surface and mid-water
853 sources of organic carbon by photoautotrophic and chemoautotrophic production in the Black
854 Sea. Deep Sea Research Part II: Topical Studies in Oceanography, 53(17-19), 1988–2004.
855 https://doi.org/10.1016/j.dsr2.2006.03.015
856
857
858 **Figure captions**
859 Fig. 1. Sampling positions of Argo floats operating from March 2005-December 2018.
860 Different colors correspond to individual floats (see the identification numbers in the legend
861 in the inset in the upper-right corner). The inset in the upper-left corner shows the number of
862 simultaneously operating floats. “V, E, B and S” show the approximate positions of the Varna
863 station, the location from which data from ERA-5 are used in the analysis, the Bosporus Strait
864 and the Sakarya River, respectively. The two triangle symbols to the east of the Sakarya River
865 show the positions of profiles measured by float 1901200 (cycle #10 on January 30 and cycle
866 #11 on February 4).
867 Fig. 2. (a) Surface air temperature at the Varna station from three-hourly data (gray line). The
868 solid black line indicates the average monthly values of the air temperature from the ERA-5
869 climatic reanalysis at the location with coordinates (32°E, 43.5°N). The two locations are
870 shown in Fig. 1. (b) Monthly mean temperature during the coldest month at the Varna station.
871 Fig. 3. Upper panels show vertical profiles of temperature (a), salinity (b) and density (c) in
872 the upper ocean (light gray isolines). Superimposed are averages for profiles from three

873 periods (see legend). The basin-averaged temperature at 50 m during the survey in July 1992
874 is shown with the triangle symbol. The temperature at the same depth from Akvanavt cruise
875 20 in December 2000 is shown with the circle symbol. The vertical line in (a) denotes a
876 temperature of 9°C. Bottom panels show the mean temperature (d) salinity (e) and density (f)
877 in the interior basin (depths larger than 1500 m, solid lines) and coastal ocean (depths less
878 than 300 m, dashed lines) for the whole period of observation.
879 Fig. 4. Time versus depth (top) and versus density (bottom) diagrams of temperature (a, e),
880 salinity (b, f) and the salinity anomaly (c, f). The mean salinity profile for the observational
881 period is subtracted in (c, f) from the current salinity. The vertical markers of the x-axes
882 correspond to January 1 of each year. The light gray isolines in (d) are isotherms 8.7 and
883 20°C. White areas indicate no (or poor) data.
884 Fig. 5. Temperature (left), salinity (middle), and σ_t (right) for selected depths. To better show
885 the joint effect of temperature and salinity, their product from which the time-averaged
886 product is subtracted is shown in (i).
887 Fig. 6. T-S (a), T- σ_t (b) and S- σ_t (c) diagrams. The corresponding times of observations are
888 shown with colors (see color bar). Isolines of σ_t, S and T are plotted in (a), (b) and (c),
889 respectively.
890 Fig. 7. Temporal evolution of T-S pairs from each profile at three σ_t levels: (a) - σ_t = 14.5; (b)
891 - σ_t = 15; (c) σ_t = 15.5. The slopes of dotted lines correspond to the respective T-S ranges,
892 which are 6.4 to 9.9 and 18.58 to 19.08 for (a); 6.4 to 9.9 and 19.22 to 19.73 for (b); and 7.9 to
893 9.1 and 20.06 to 20.24 for (c).
894

Figure_01.

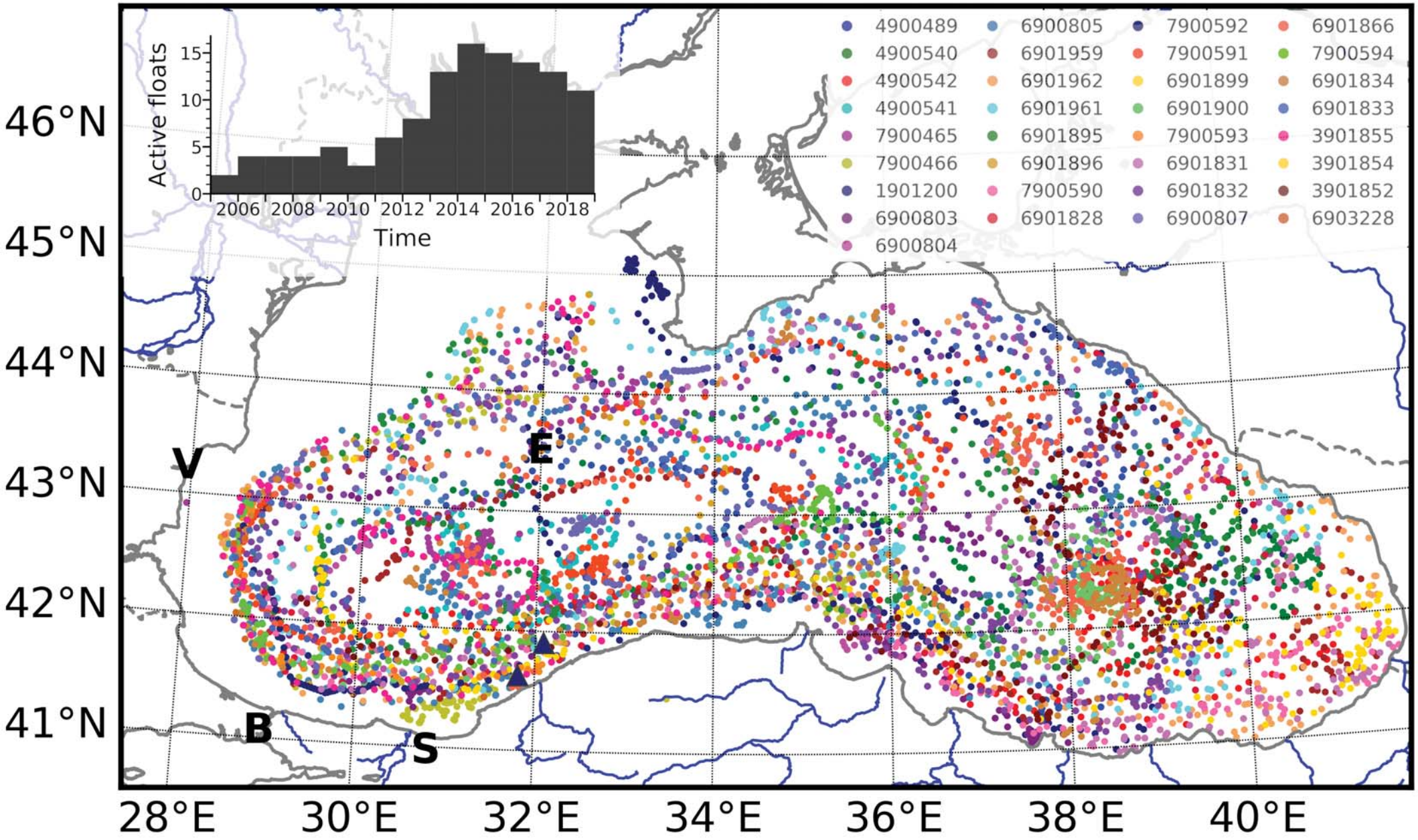
Active floats
15
10
5
0
2006 2008 2010 2012 2014 2016 2018
Time
4900489
4900540
4900542
4900541
7900465
7900466
1901200
6900803
6900804
6900805
6901959
6901962
6901961
6901895
6901896
7900590
6901828
7900592
7900591
6901899
6901900
7900593
6901831
6901832
6900807
6901866
7900594
6901834
6901833
3901855
3901854
3901852
6903228
46°N
45°N
44°N
43°N
42°N
41°N
28°E
30°E
32°E
34°E
36°E
38°E
40°E
V
E
B
S

Figure_02.

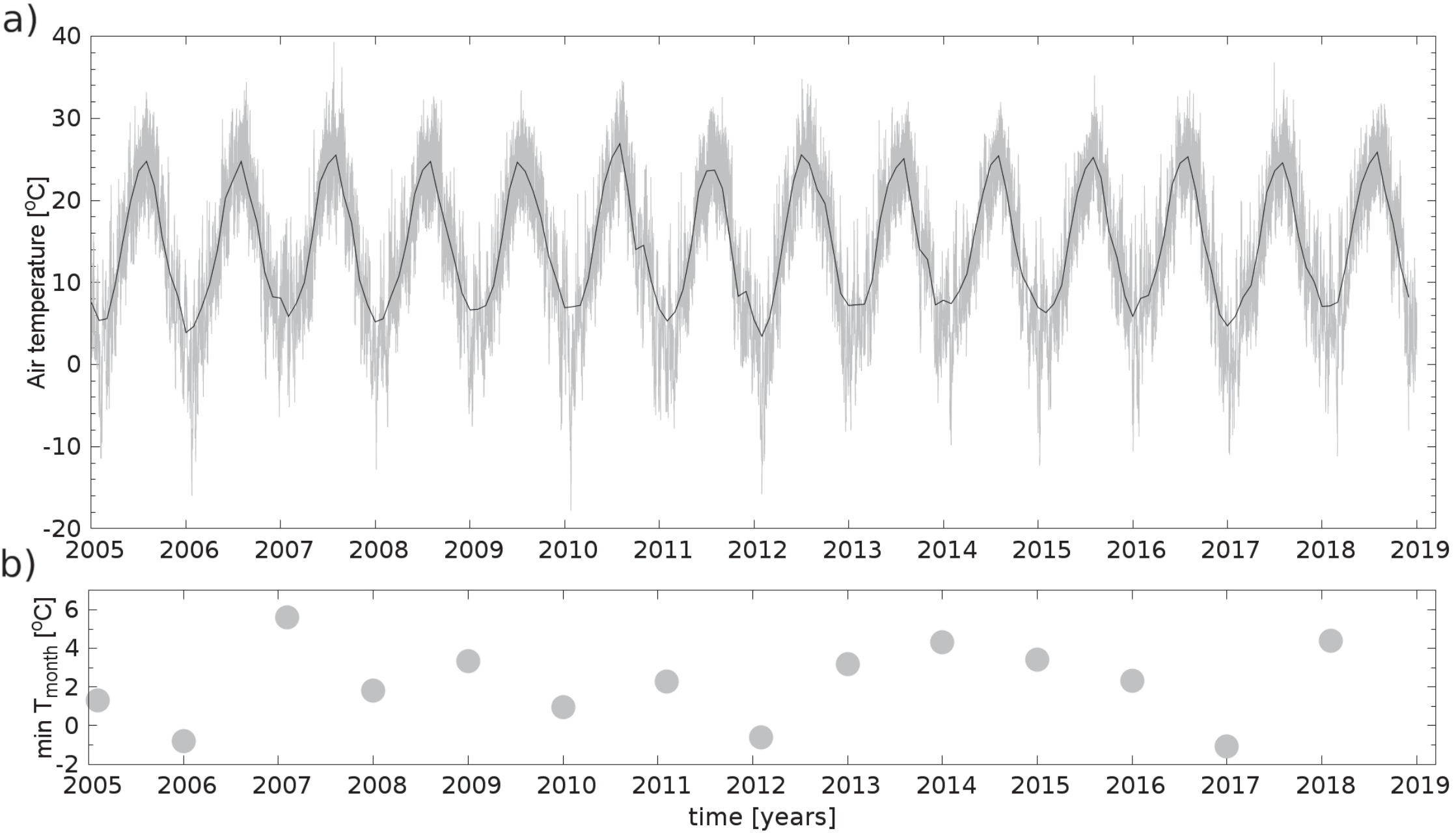
a)
Air temperature [°C]
40
30
20
10
0
-10
-20
2005
2006
2007
2008
2009
2010
2011
2012
2013
2014
2015
2016
2017
2018
2019
b)
min T_month [°C]
6
4
2
0
-2
time [years]

Figure_03.

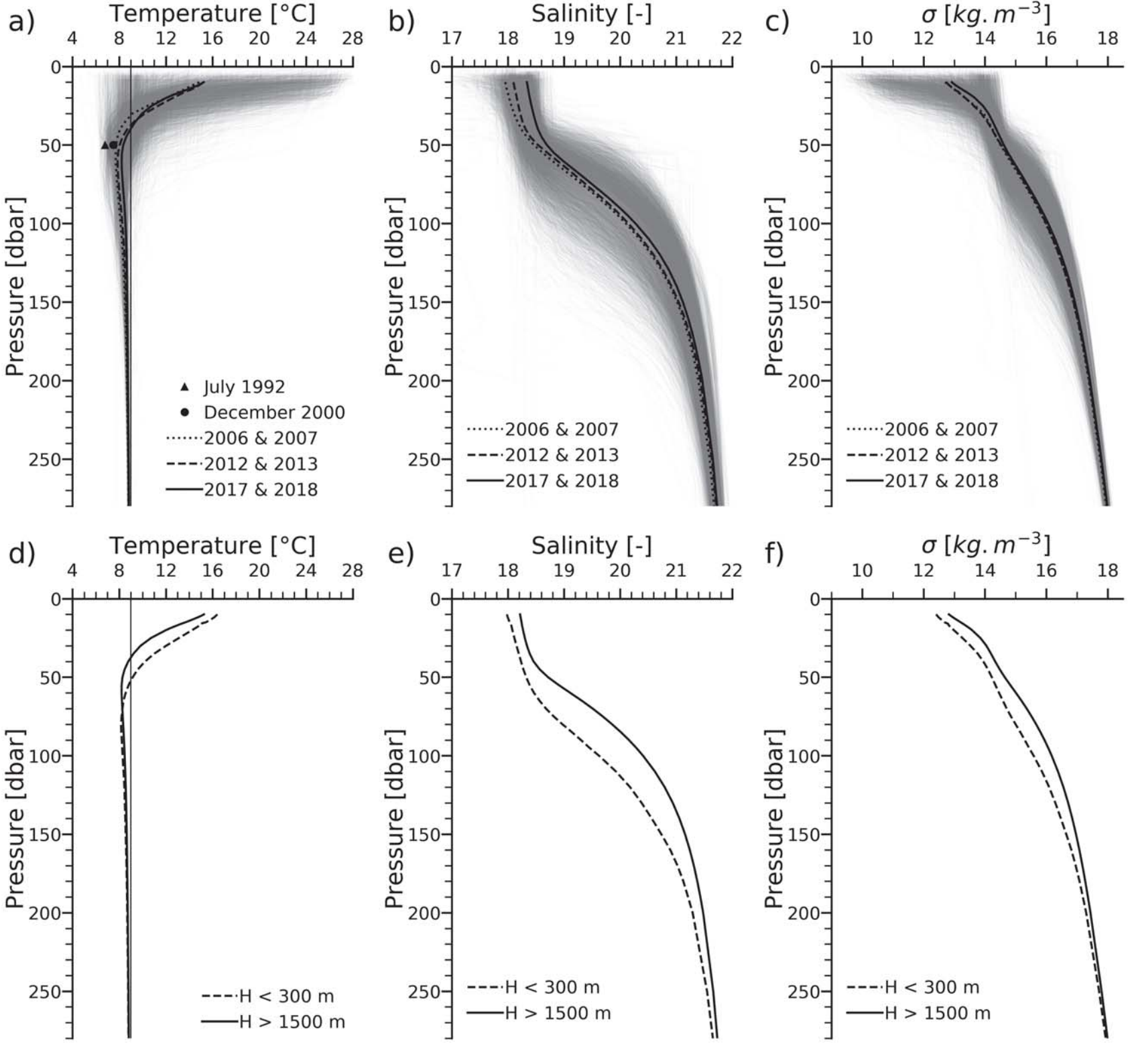
a)
Temperature [°C]
4 8 12 16 20 24 28
Pressure [dbar]
0 50 100 150 200 250
July 1992
December 2000
2006 & 2007
2012 & 2013
2017 & 2018
b)
Salinity [-]
17 18 19 20 21 22
Pressure [dbar]
0 50 100 150 200 250
2006 & 2007
2012 & 2013
2017 & 2018
c)
σ [kg. m−3]
10 12 14 16 18
Pressure [dbar]
0 50 100 150 200 250
2006 & 2007
2012 & 2013
2017 & 2018
d)
Temperature [°C]
4 8 12 16 20 24 28
Pressure [dbar]
0 50 100 150 200 250
H < 300 m
H > 1500 m
e)
Salinity [-]
17 18 19 20 21 22
Pressure [dbar]
0 50 100 150 200 250
H < 300 m
H > 1500 m
f)
σ [kg. m−3]
10 12 14 16 18
Pressure [dbar]
0 50 100 150 200 250
H < 300 m
H > 1500 m

Figure_04.

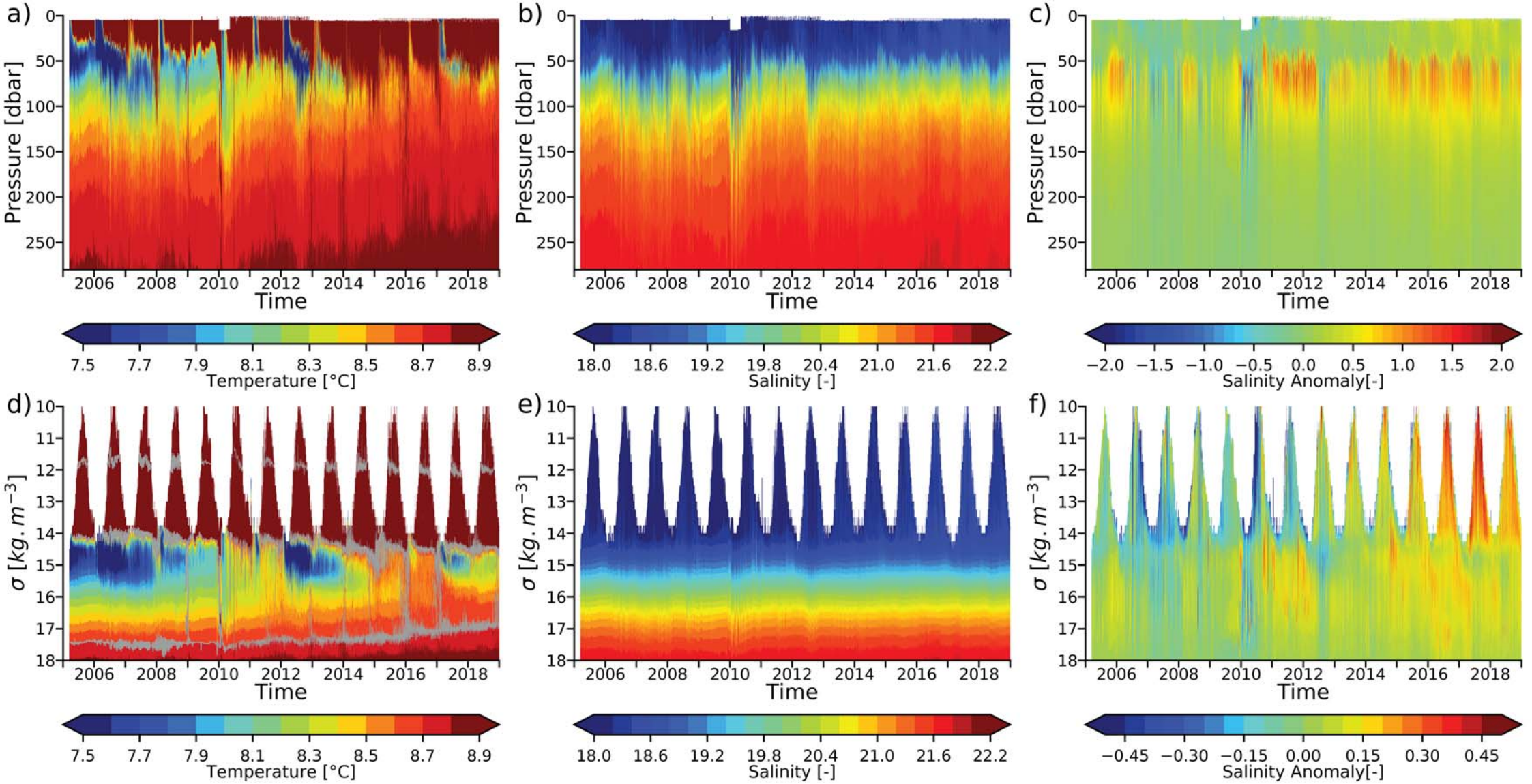
a)
b)
c)
d)
e)
f)
Pressure [dbar]
σ [kg.m⁻³]
Time
2006 2008 2010 2012 2014 2016 2018
Temperature [°C]
7.5 7.7 7.9 8.1 8.3 8.5 8.7 8.9
Salinity [-]
18.0 18.6 19.2 19.8 20.4 21.0 21.6 22.2
Salinity Anomaly[-]
−2.0 −1.5 −1.0 −0.5 0.0 0.5 1.0 1.5 2.0
−0.45 −0.30 −0.15 0.00 0.15 0.30 0.45

Figure_05.

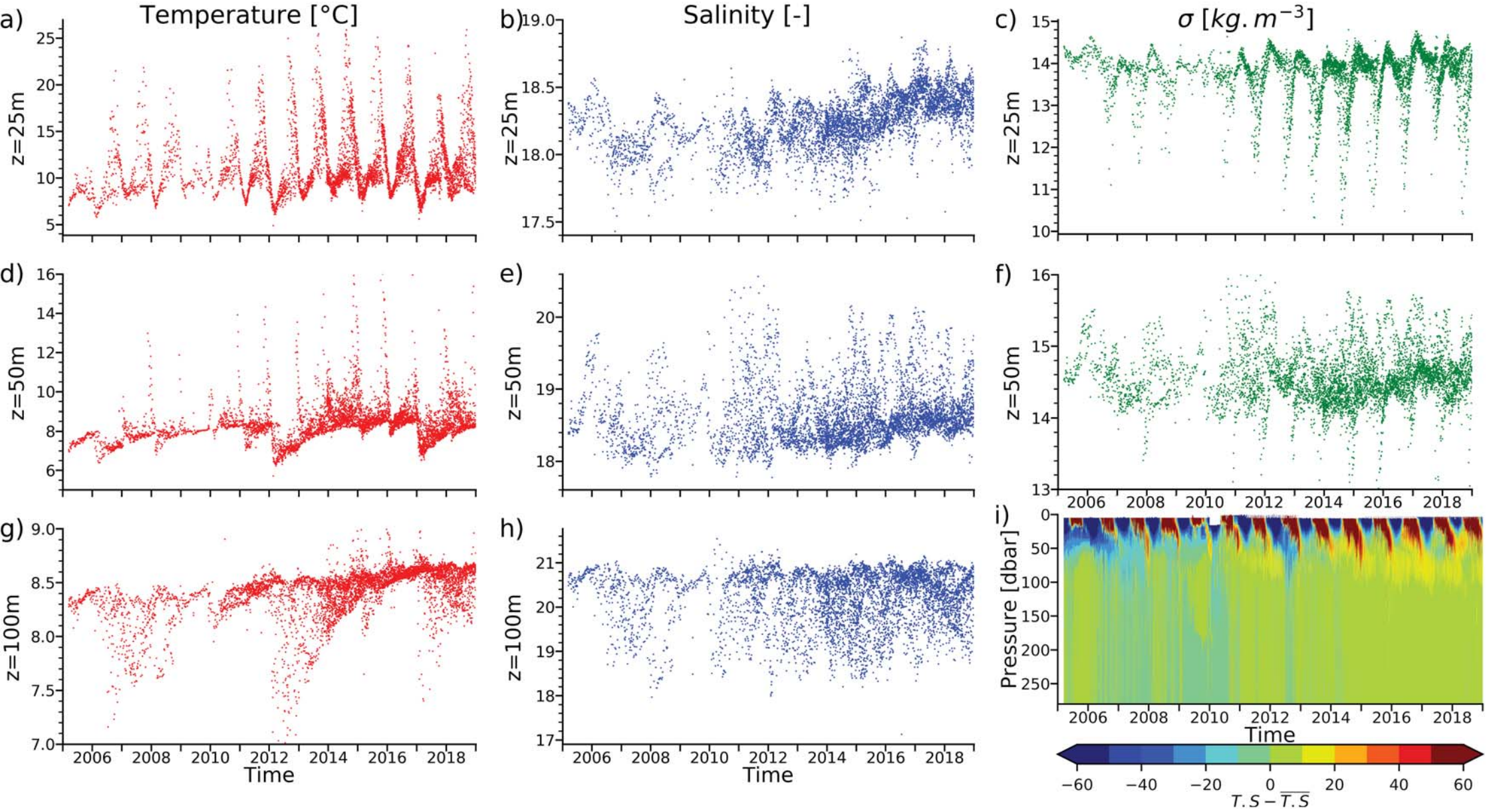
a)
Temperature [°C]
z=25m
b)
Salinity [-]
z=25m
c)
σ [$kg.m^{-3}$]
z=25m
d)
z=50m
e)
z=50m
f)
z=50m
g)
z=100m
h)
z=100m
i)
Pressure [dbar]
Time
Time
Time
$T.S - \overline{T.S}$

Figure_06.

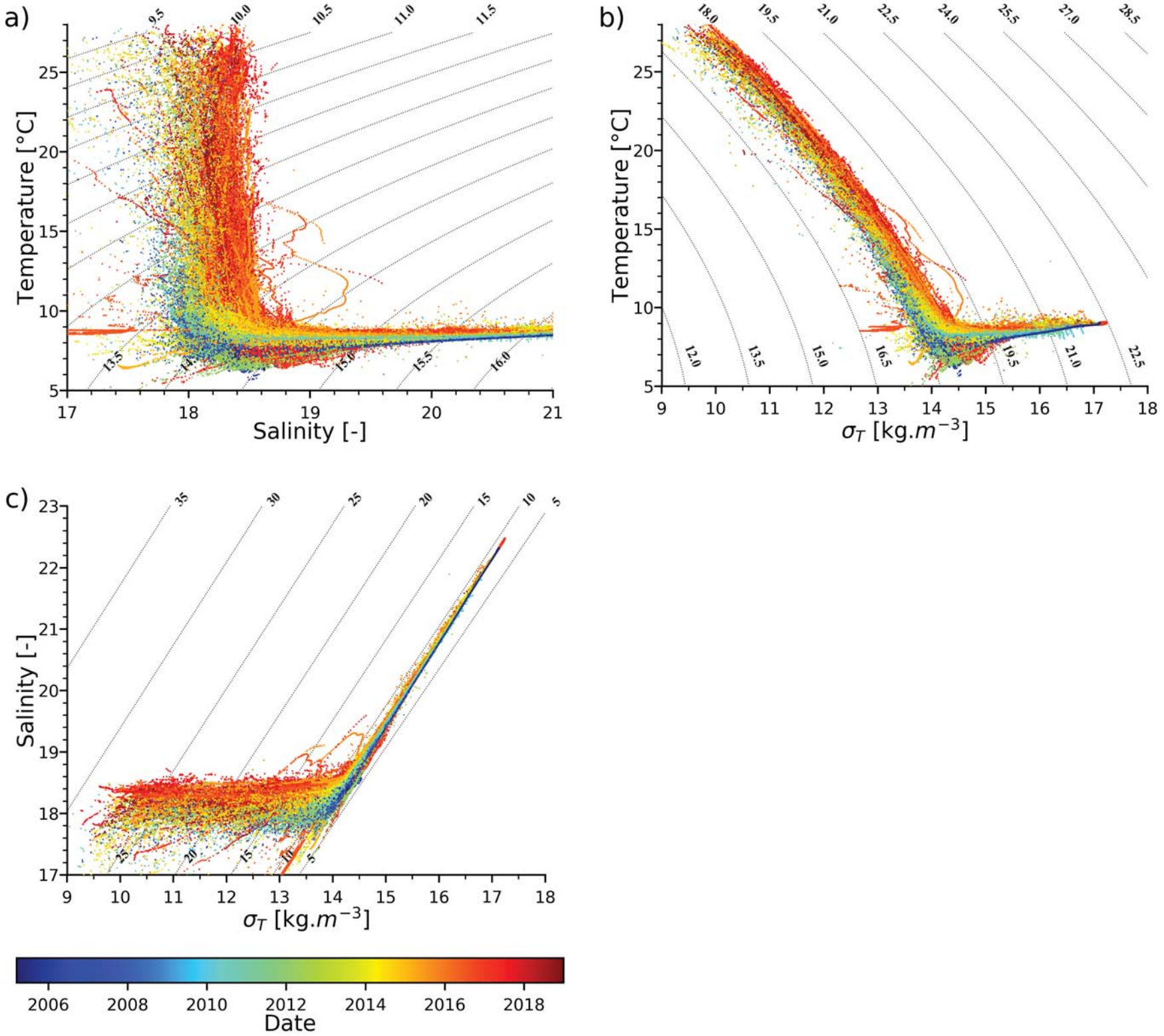
a)
Temperature [°C]
Salinity [-]
b)
Temperature [°C]
σ_T [kg.m^{-3}]
c)
Salinity [-]
σ_T [kg.m^{-3}]
Date
2006
2008
2010
2012
2014
2016
2018

Figure_07.

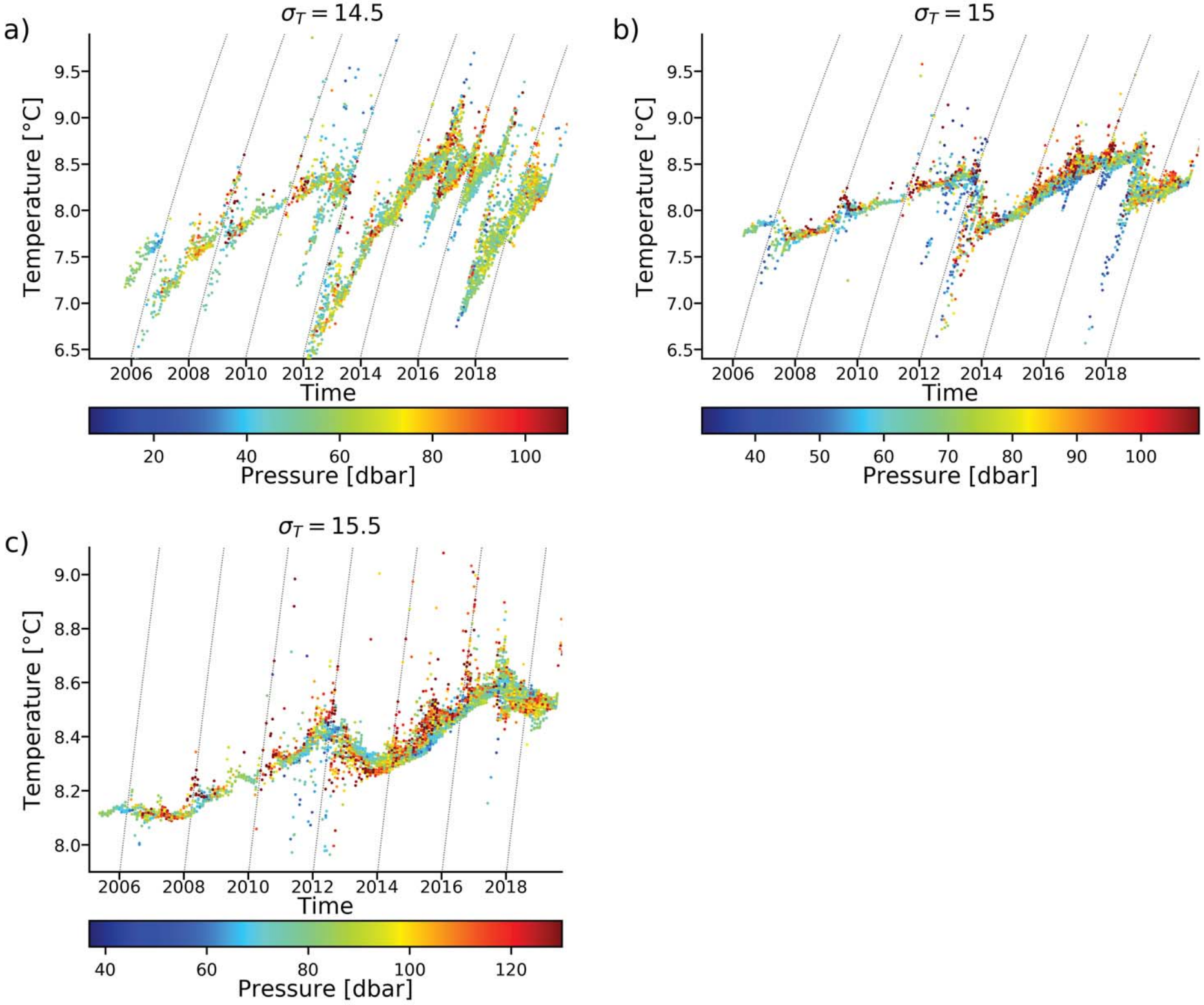
a)
$\sigma_T = 14.5$
Temperature [°C]
9.5
9.0
8.5
8.0
7.5
7.0
6.5
2006
2008
2010
2012
2014
2016
2018
Time
20
40
60
80
100
Pressure [dbar]
b)
$\sigma_T = 15$
Temperature [°C]
9.5
9.0
8.5
8.0
7.5
7.0
6.5
2006
2008
2010
2012
2014
2016
2018
Time
40
50
60
70
80
90
100
Pressure [dbar]
c)
$\sigma_T = 15.5$
Temperature [°C]
9.0
8.8
8.6
8.4
8.2
8.0
2006
2008
2010
2012
2014
2016
2018
Time
40
60
80
100
120
Pressure [dbar]